

Supplemental figures

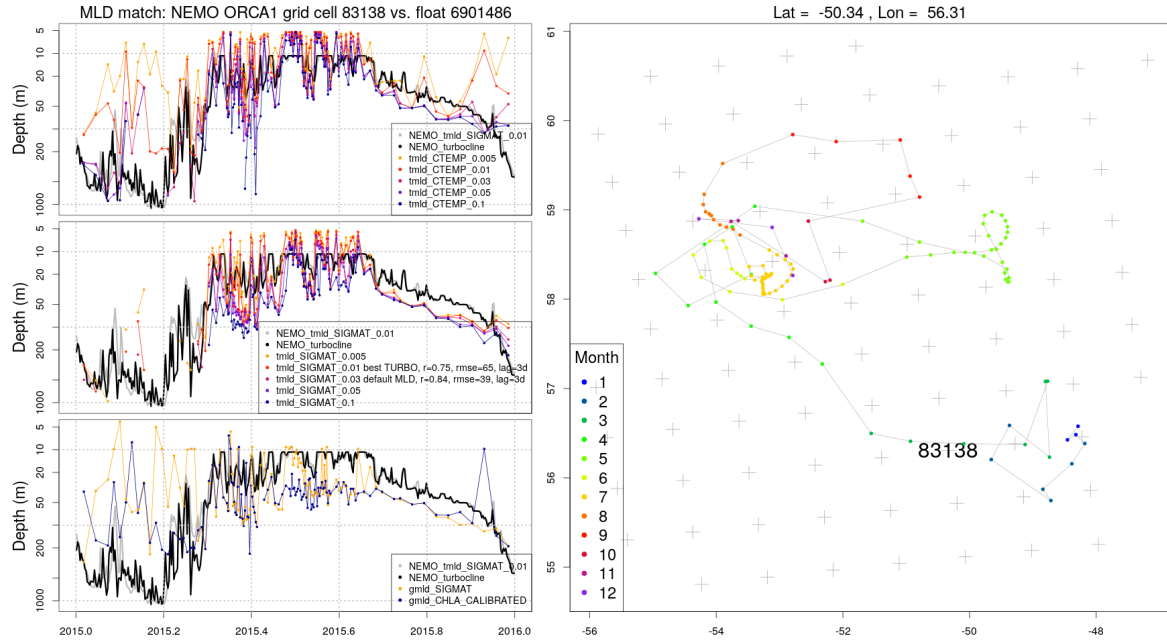


Figure S1. Comparison of NEMO turbocline depth in one model cell (83138) and the MLD recorded by a BGC-Argo float over one year. Observed MLD is estimated with 12 different metrics: temperature thresholds of 0.005, 0.01, 0.03, 0.05 and 0.1 °C from 5 m (top left); density thresholds of 0.005, 0.01, 0.03, 0.05 and 0.1 kg m⁻³ from 5 m (center left); and highest density and Chla fluorescence gradients (bottom left). A density threshold of 0.03 kg m⁻³ from the 5-m reference depth is used as the default criterion to evaluate the comparison with different skill metrics. This figure corresponds to float WMO 6901486 in the Labrador Sea, year 2015, compared to model grid cell 83138 (Fig. 6 of the main text). The gaps in the MLD lines for BGC-Argo observations indicate that the MLD was deeper than 1000 m for a given MLD criterion. Only the finest MLD criteria detected stratification shallower than 1000 m during the winter convection season (approximately, February and March). Analogous figures were made for all the model grid cells visited by the float (shown in the right panel) and used to compute the corresponding MLD skill metrics (Fig. S2-S4), for all the coherent annual time series (CATS).

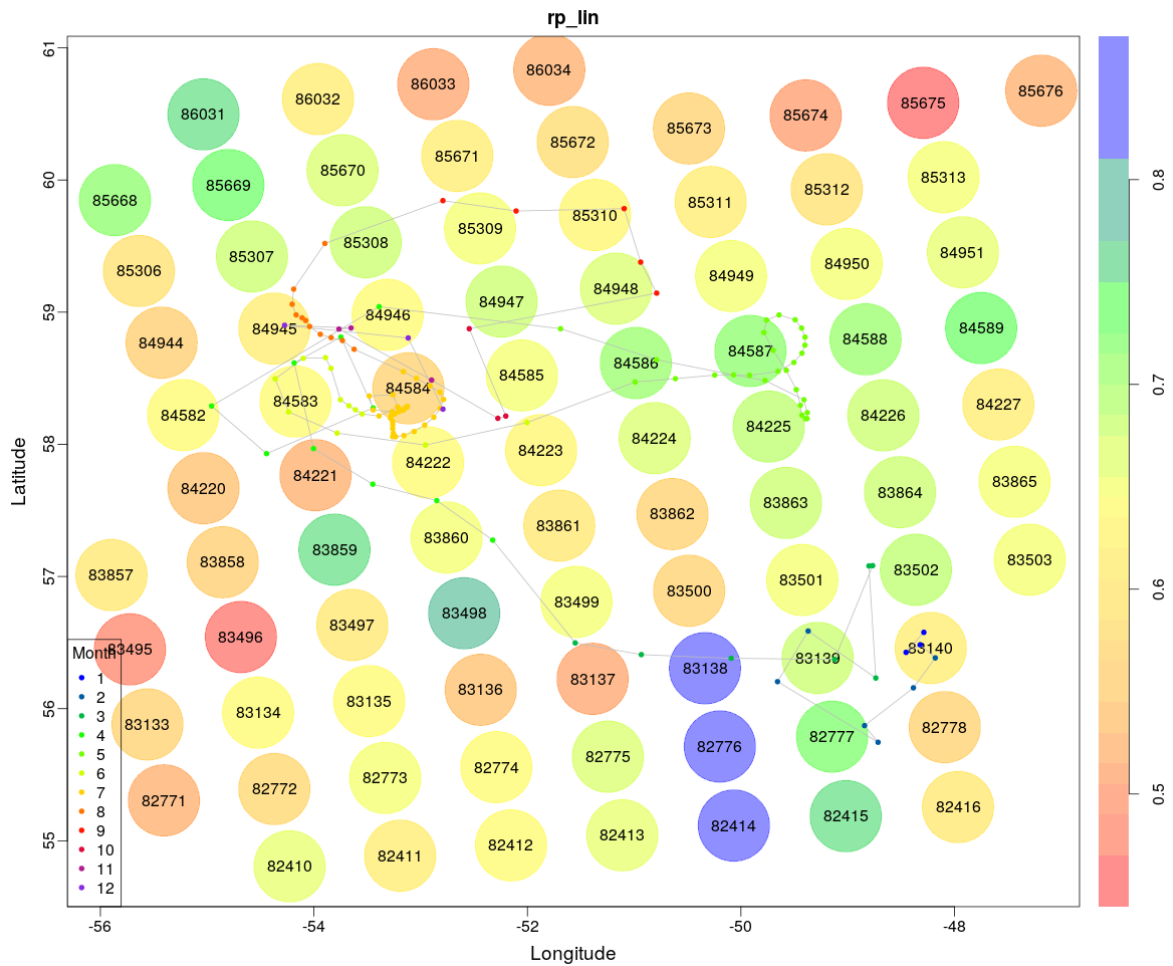


Figure S2. Pearson's correlation between NEMO and BGC-Argo MLD over the annual cycle for float WMO 6901486, year 2015.

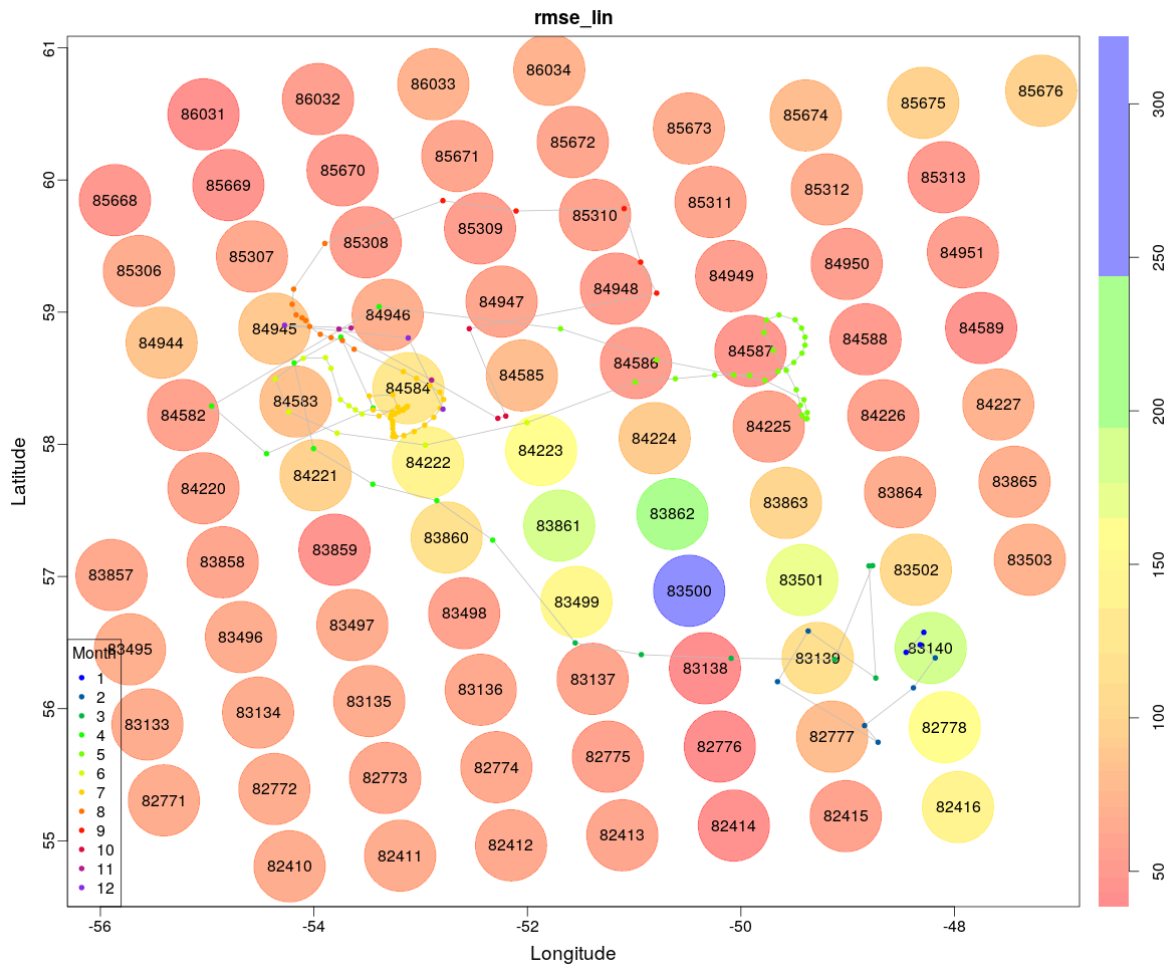


Figure S3. RMSE between NEMO and BGC-Argo MLD over the annual cycle for float WMO 6901486, year 2015.

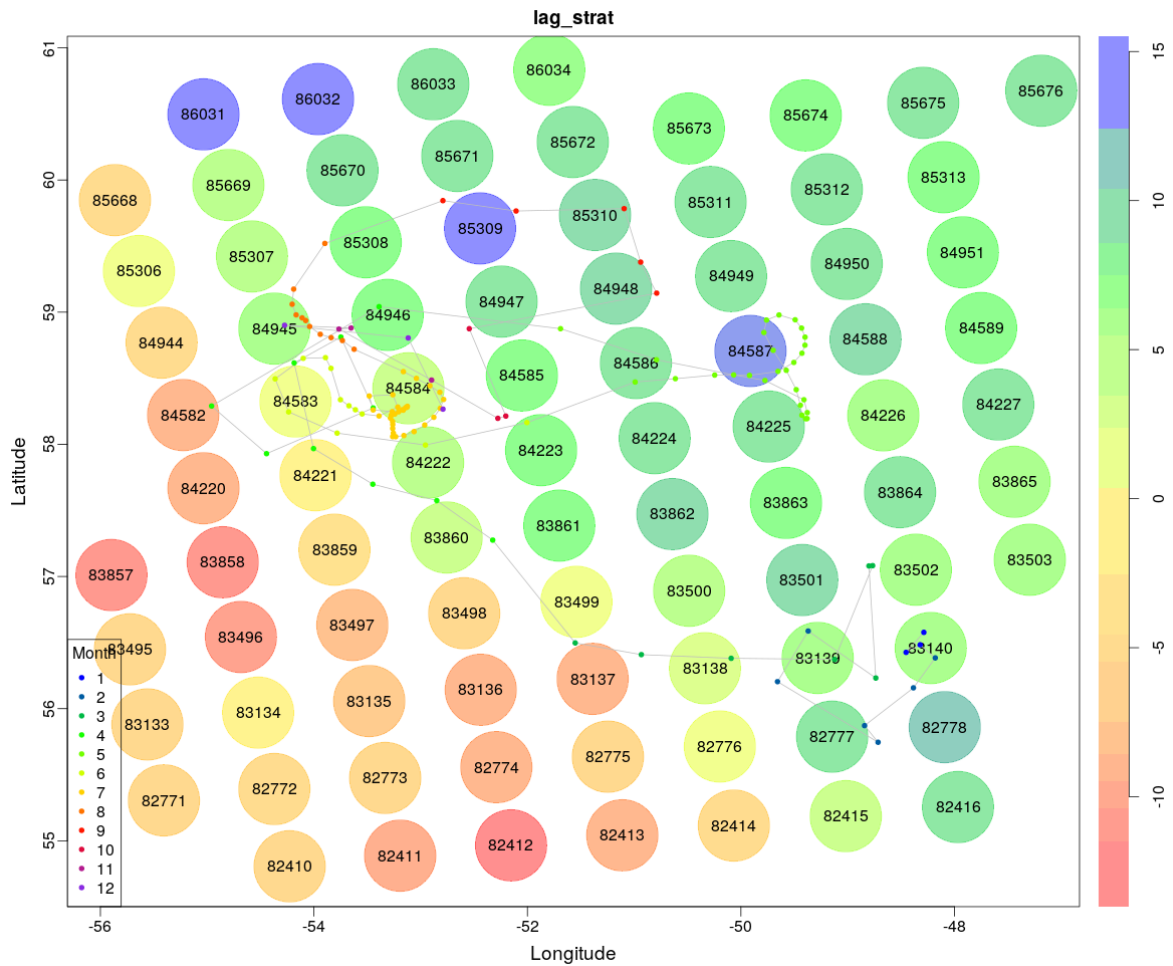


Figure S4. Time lag between the onset of permanent stratification in NEMO and BGC-Argo MLD over the annual cycle for float WMO 6901486, year 2015.

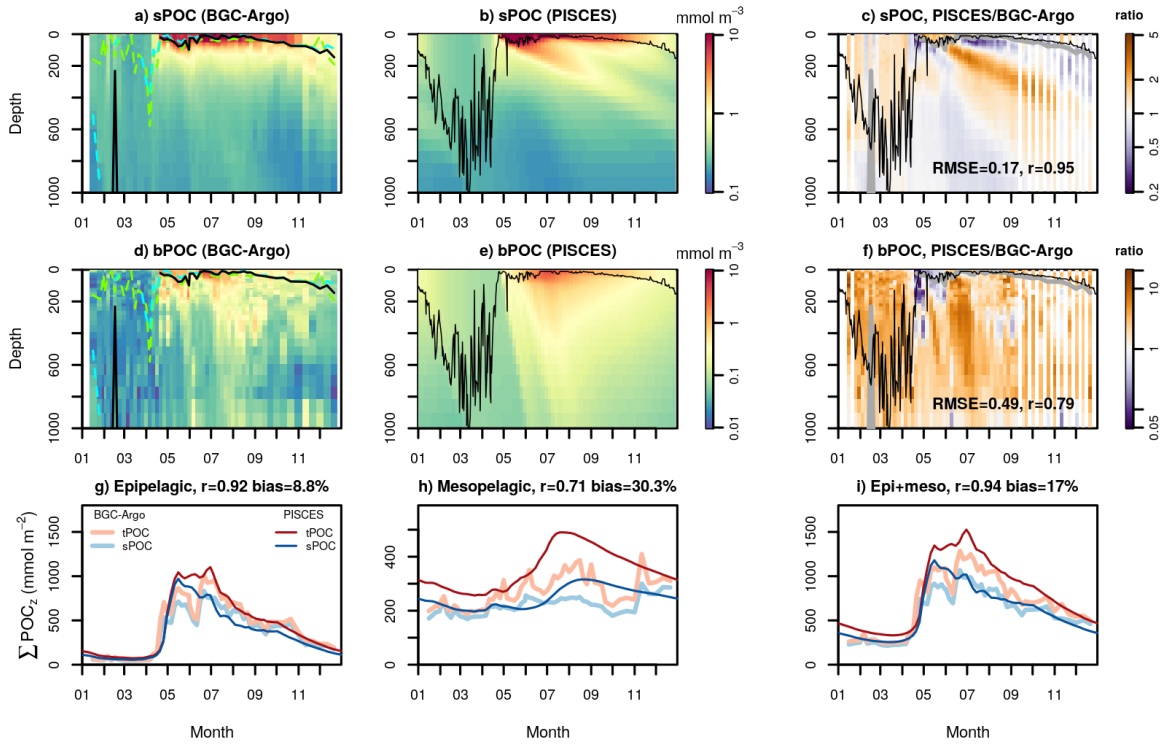


Figure S5. As Fig. 6 of the main text, with the same BGC-Argo dataset but using dynamical fields from a different model grid cell to force the PISCES 1D simulation.

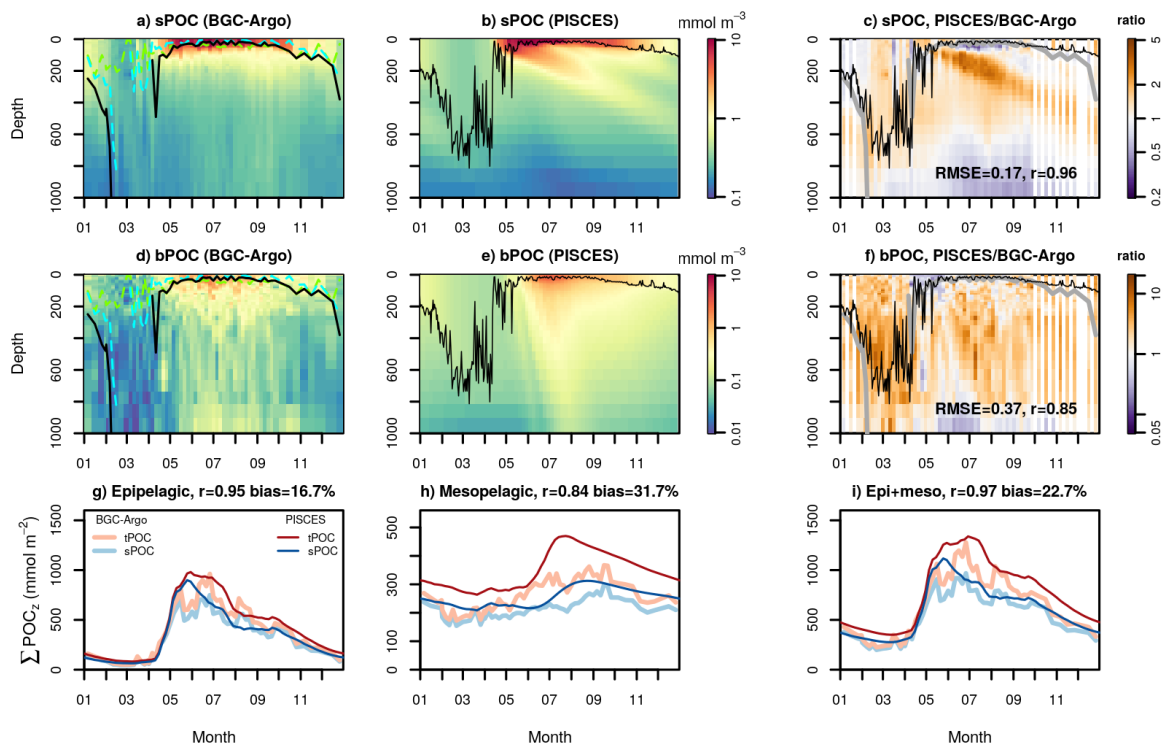


Figure S6. As Fig. 6 of the main text for float WMO 6901527, year 2016 (Labrador Sea).

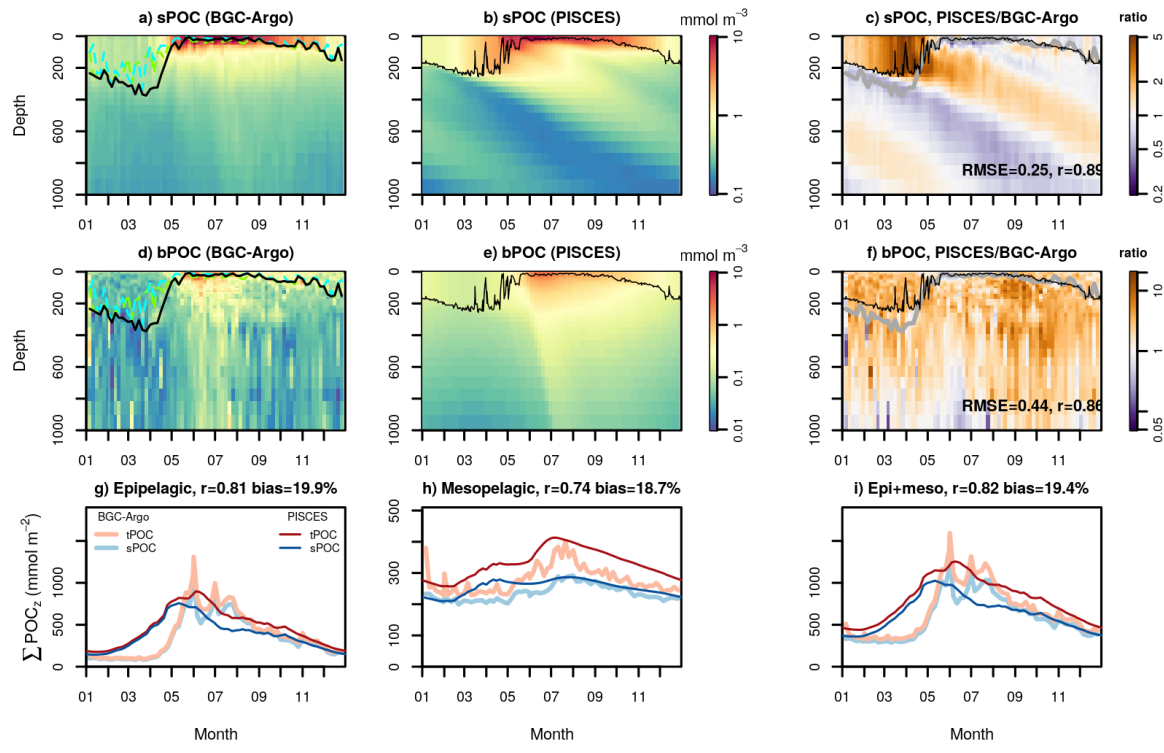


Figure S7. As Fig. 6 of the main text for float WMO 6901516, year 2014 (Iceland Basin).

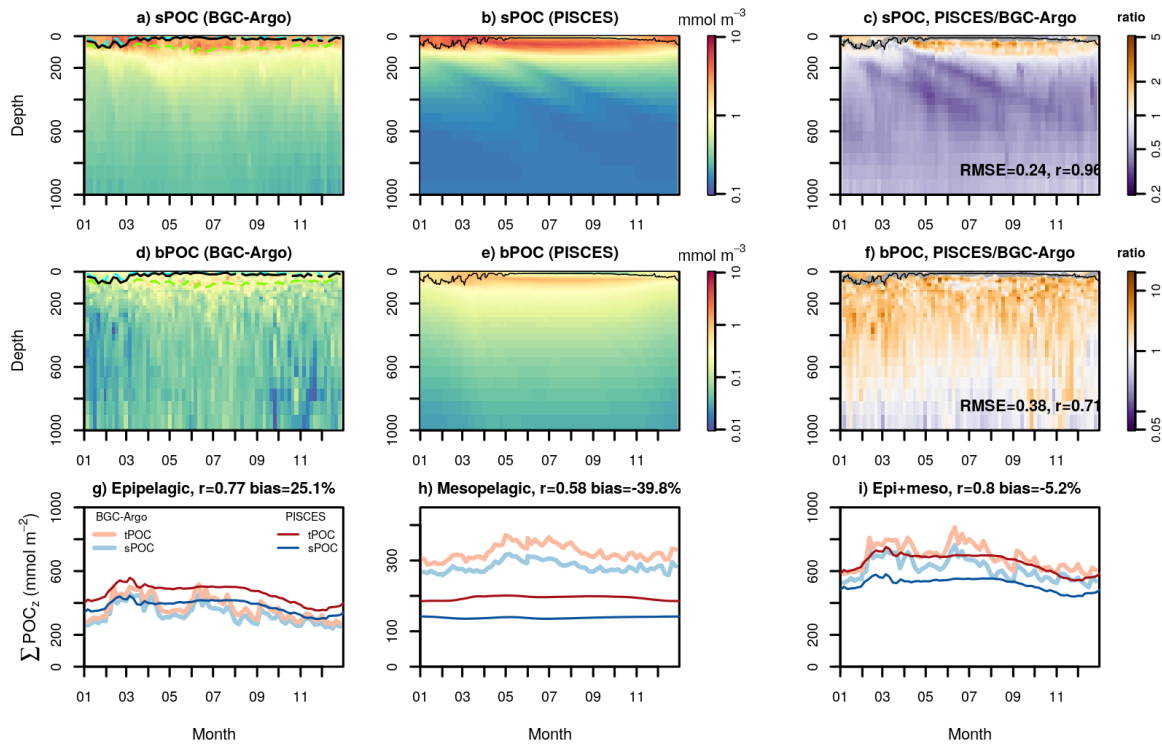


Figure S8. As Fig. 6 of the main text for float WMO 6901491, year 2014 (Tyrrhenian Sea, Mediterranean).

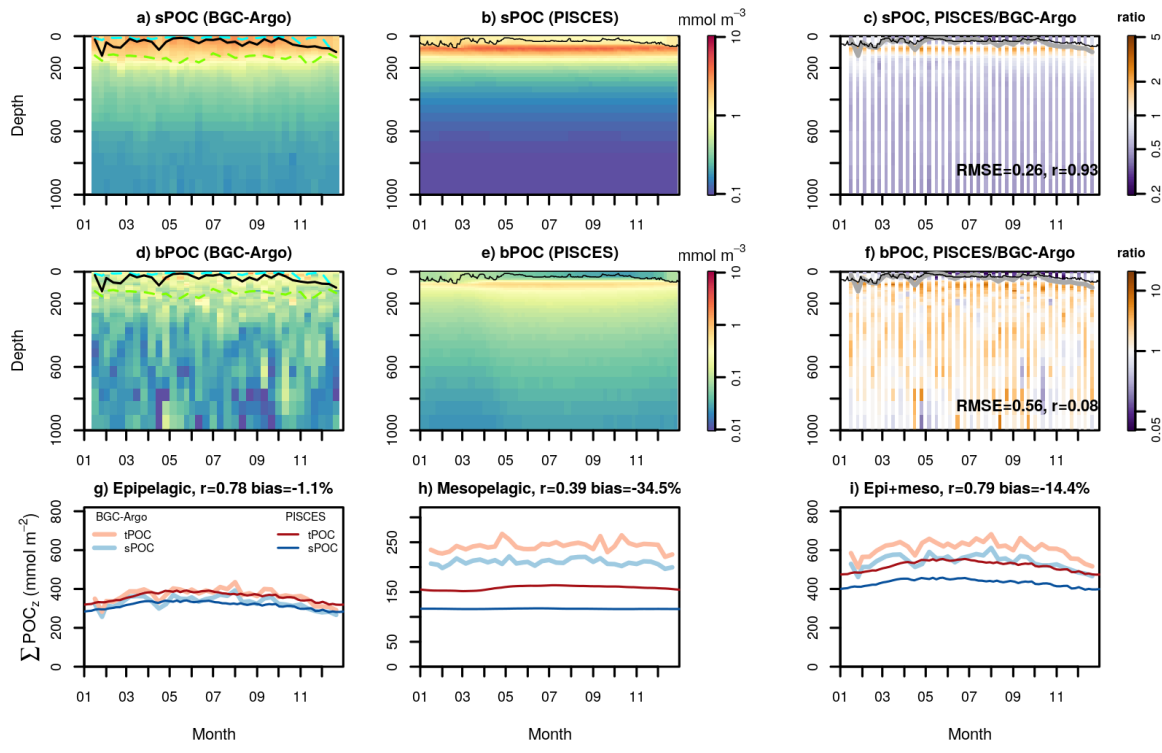


Figure S9. As Fig. 6 of the main text for float WMO 6901472, year 2013 (North Atlantic subtropical gyre).

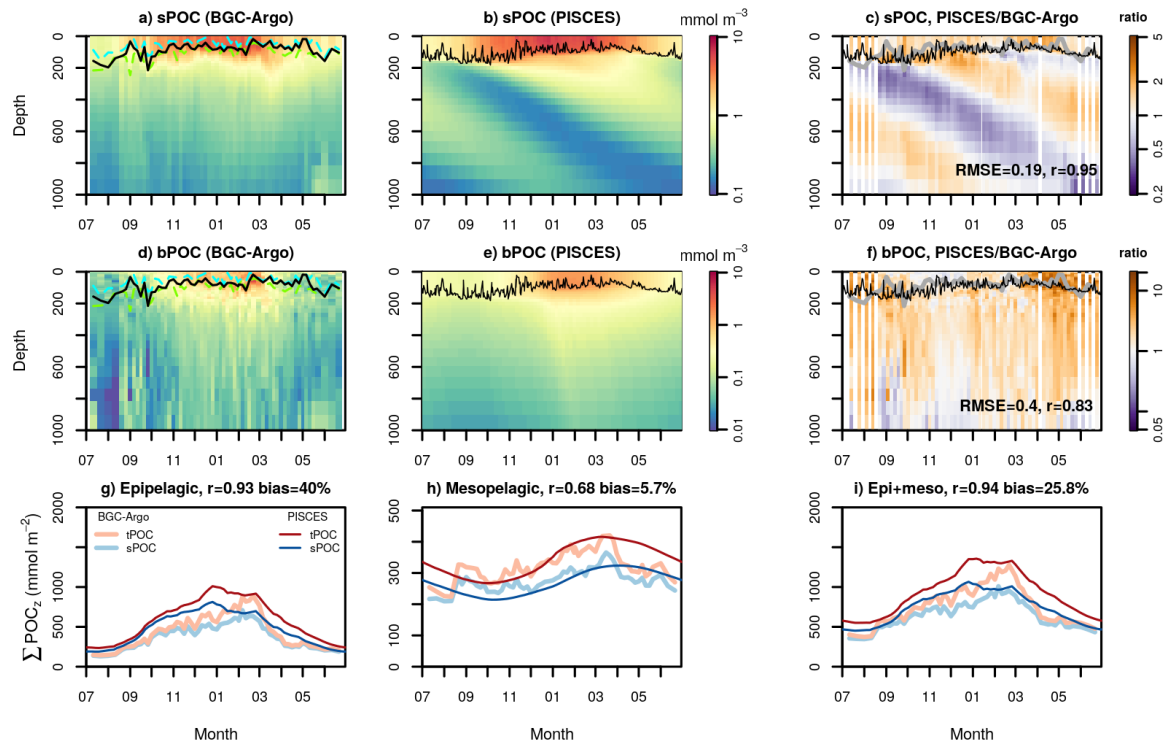


Figure S10. As Fig. 6 of the main text for float WMO 6901579, year 2015 (Indian sector of the Southern Ocean).

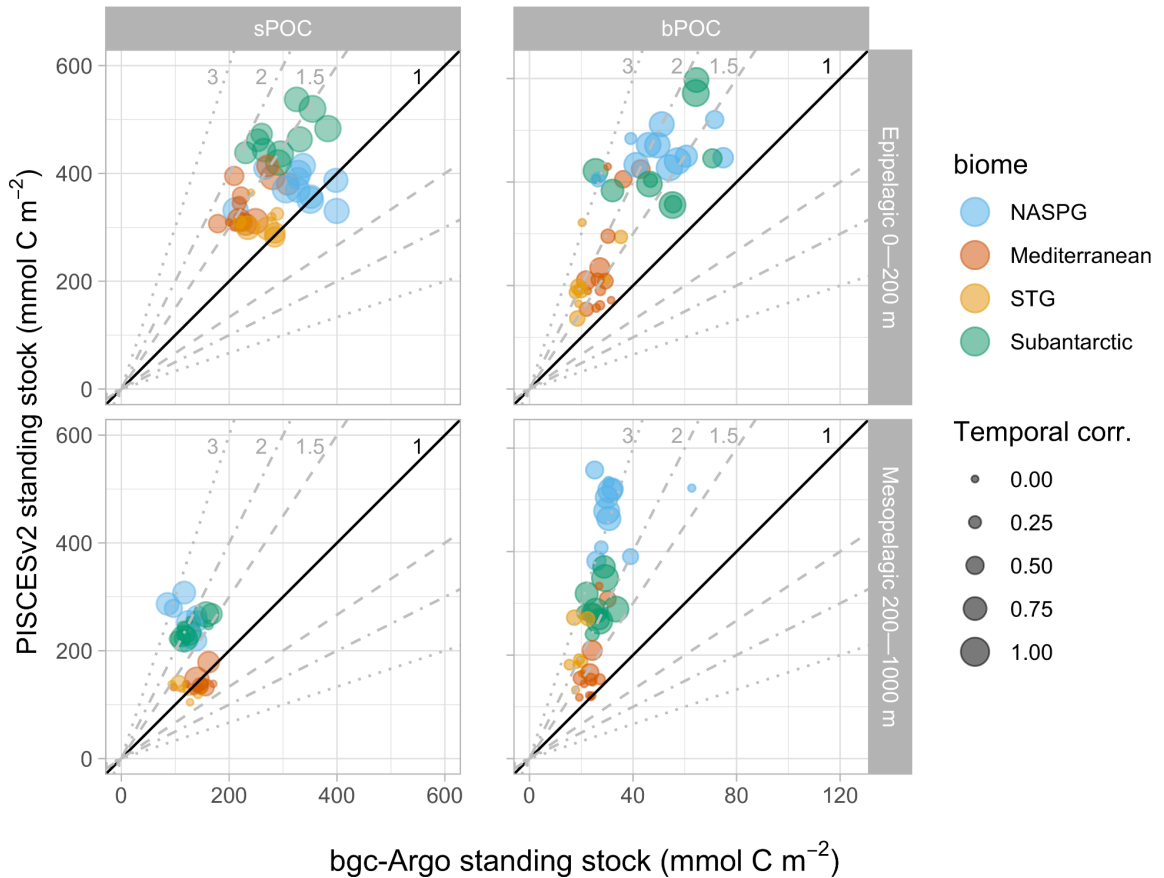


Figure S11. This figure is analogous to Figure 8 of the main paper, except that the asymptotic bbp700-POC conversion factor in deep waters (constant “c” in eq. 1) has been set to 500 mmol C m⁻² instead of 1000 mmol C m⁻². BGC-Argo versus PISCES scatterplots are shown for small POC (sPOC) and big POC (bPOC) in the epi- and mesopelagic layers. Reference lines indicate a range of model: data ratios, from 1:1 (perfect correspondence) to a factor of 3 or its inverse. Biomes are distinguished with different colors, and the size of the circles is proportional to the correlation between BGC-Argo and PISCES stocks (as shown in the bottom panels of Figures 6 and 7).

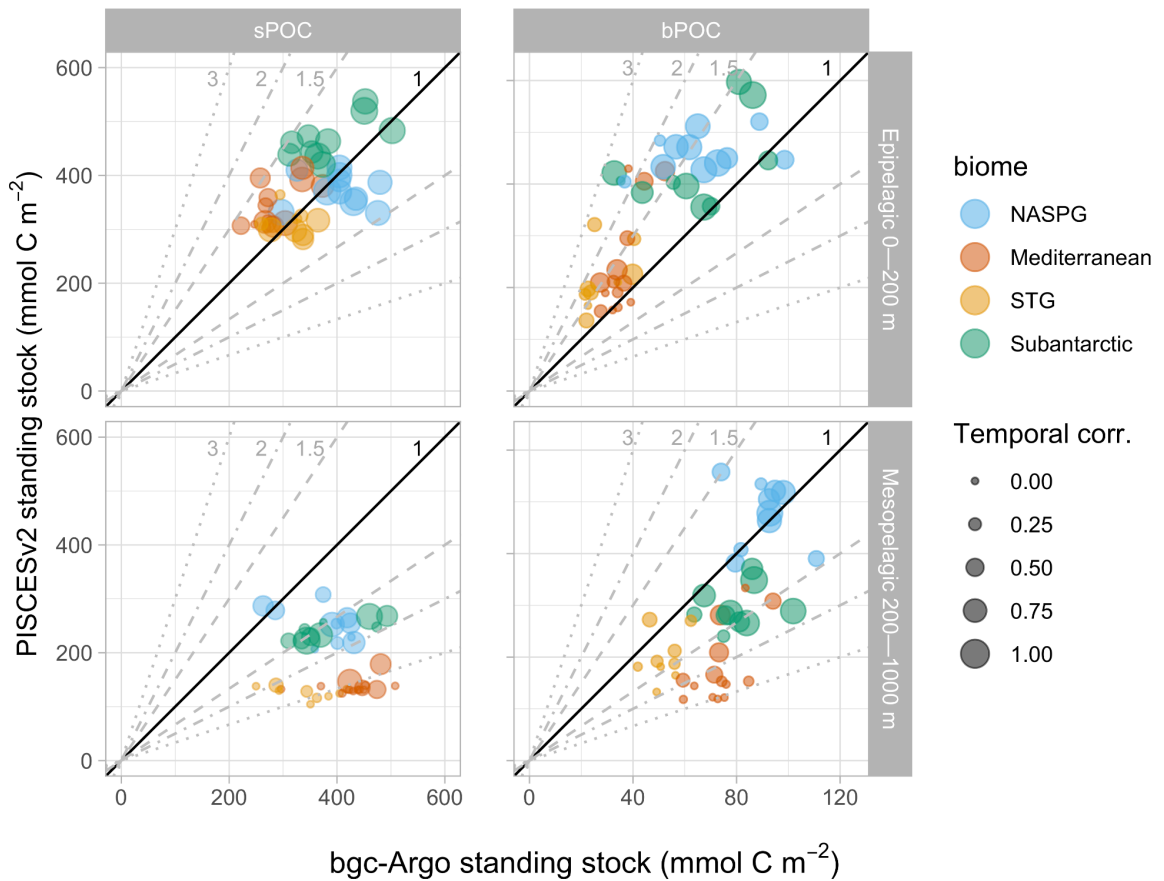


Figure S12. This figure is analogous to Figure 8 of the main paper, except that the asymptotic $bbp700$ -POC conversion factor in deep waters (constant “ c ” in eq. 1) has been set to $2000 \text{ mmol C m}^{-2}$ instead of $1000 \text{ mmol C m}^{-2}$. BGC-Argo versus PISCES scatterplots are shown for small POC (sPOC) and big POC (bPOC) in the epi- and mesopelagic layers. Reference lines indicate a range of model:data ratios, from 1:1 (perfect correspondence) to a factor of 3 or its inverse. Biomes are distinguished with different colors, and the size of the circles is proportional to the correlation between BGC-Argo and PISCES stocks (as shown in the bottom panels of Figures 6 and 7).

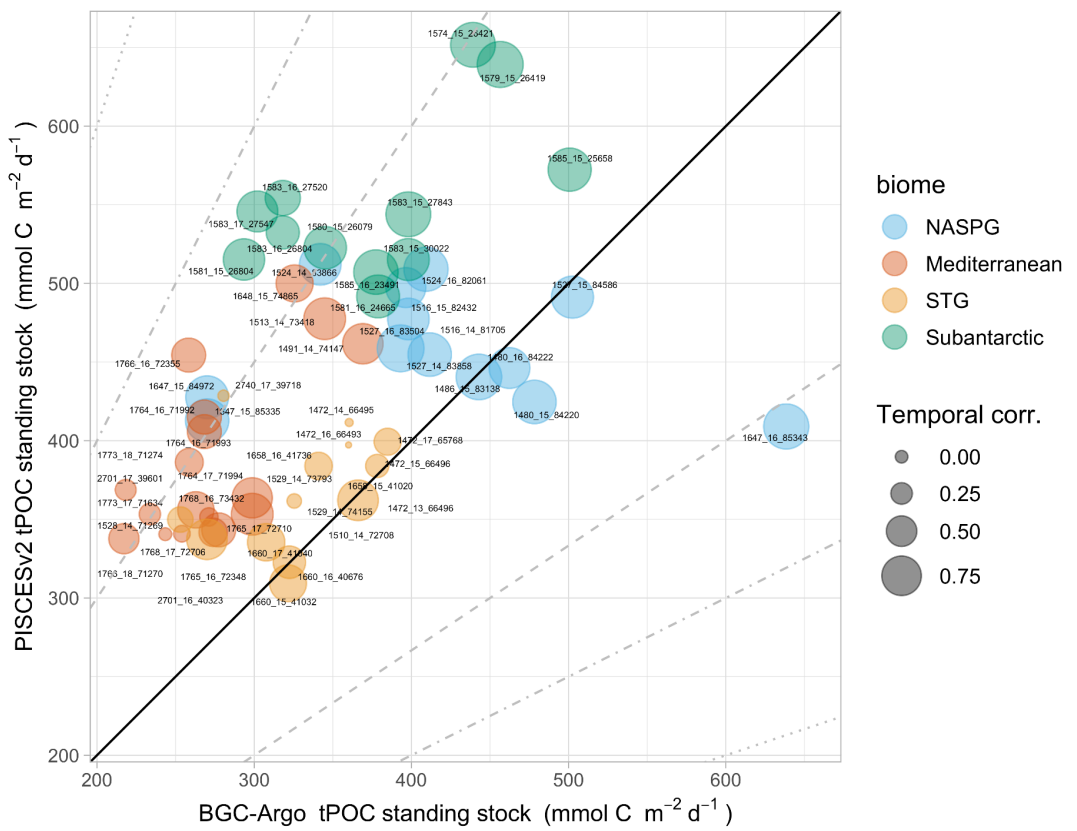


Figure S13. As top panels of Fig. 8, but showing total POC (tPOC = sPOC + bPOC) including an outlier that was discarded from the analyses shown in the main text. The outlier is float 6901647, year 2016 (labelled 1647_16_85343 on the plot).

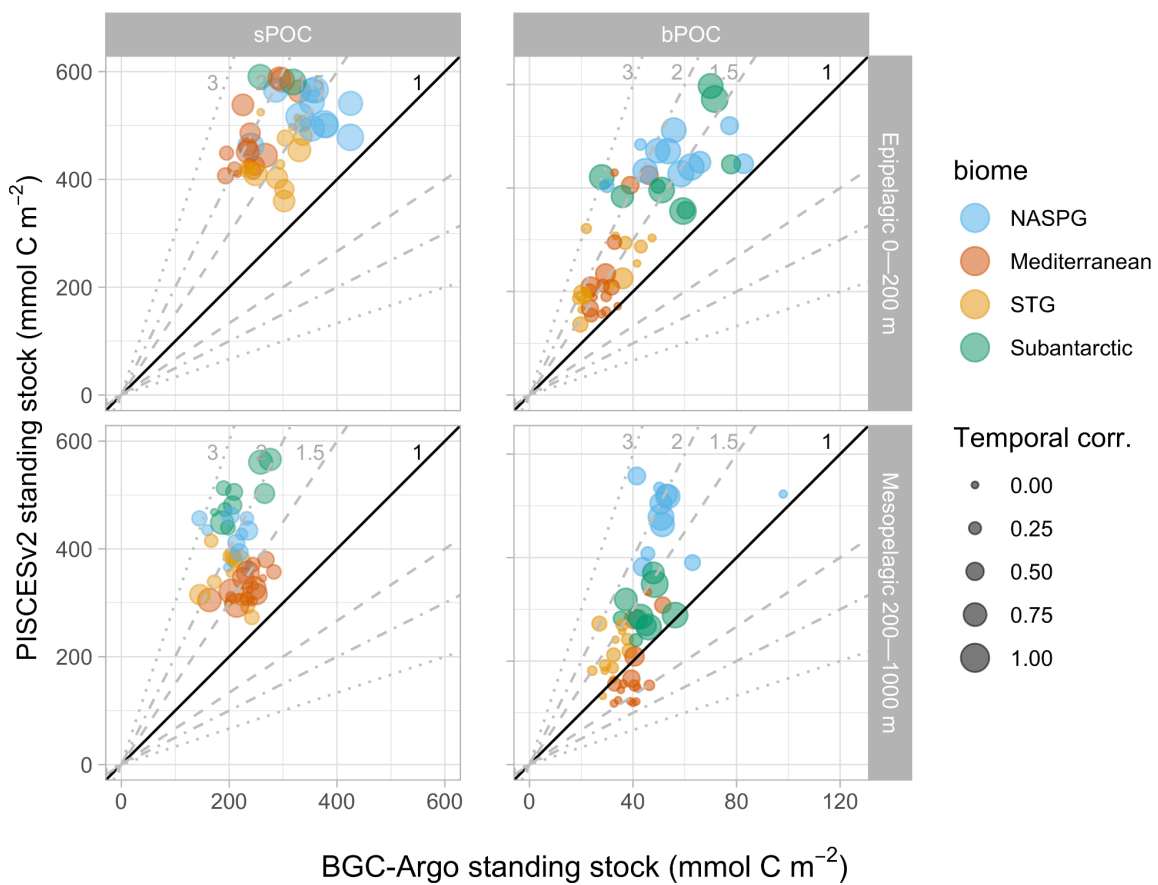


Figure S14. Alternative version of Fig. 8, including heterotrophic prokaryotes' biomass (*BACT*) diagnosed within PISCES using a simple empirical relationship.

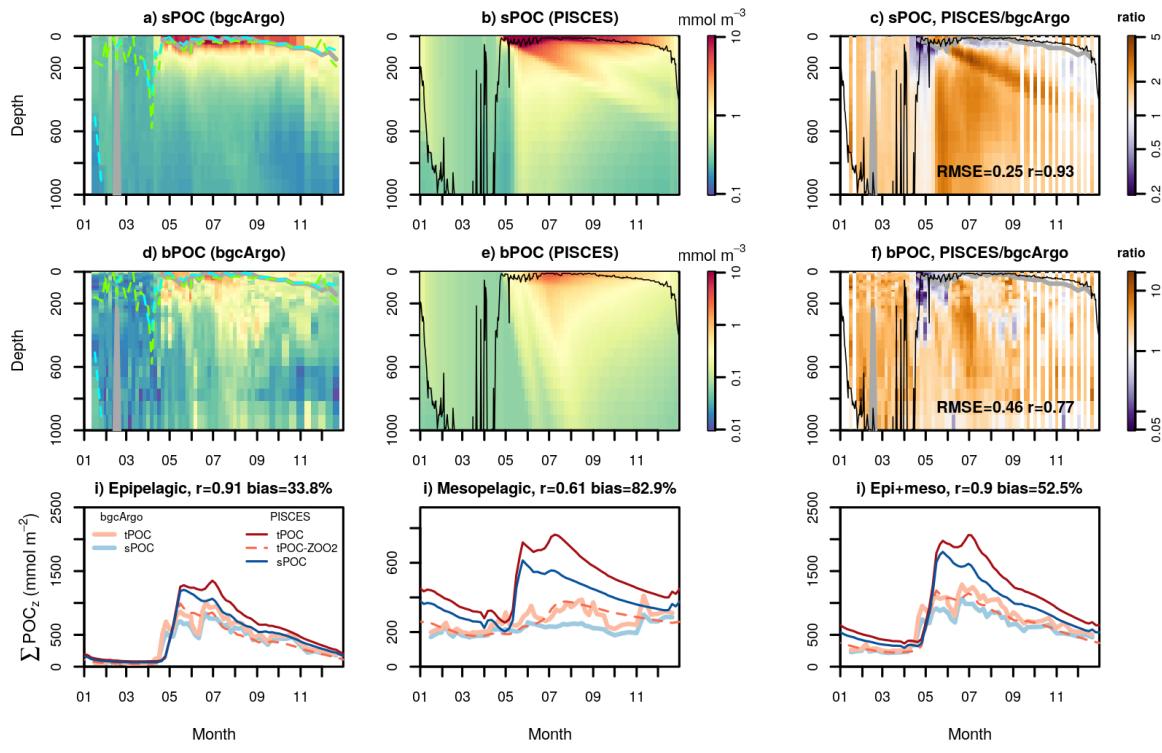


Figure S15. Alternative version of Fig. 6 of the main text including heterotrophic prokaryotes' biomass (*BACT*) diagnosed within PISCES using a simple empirical relationship.

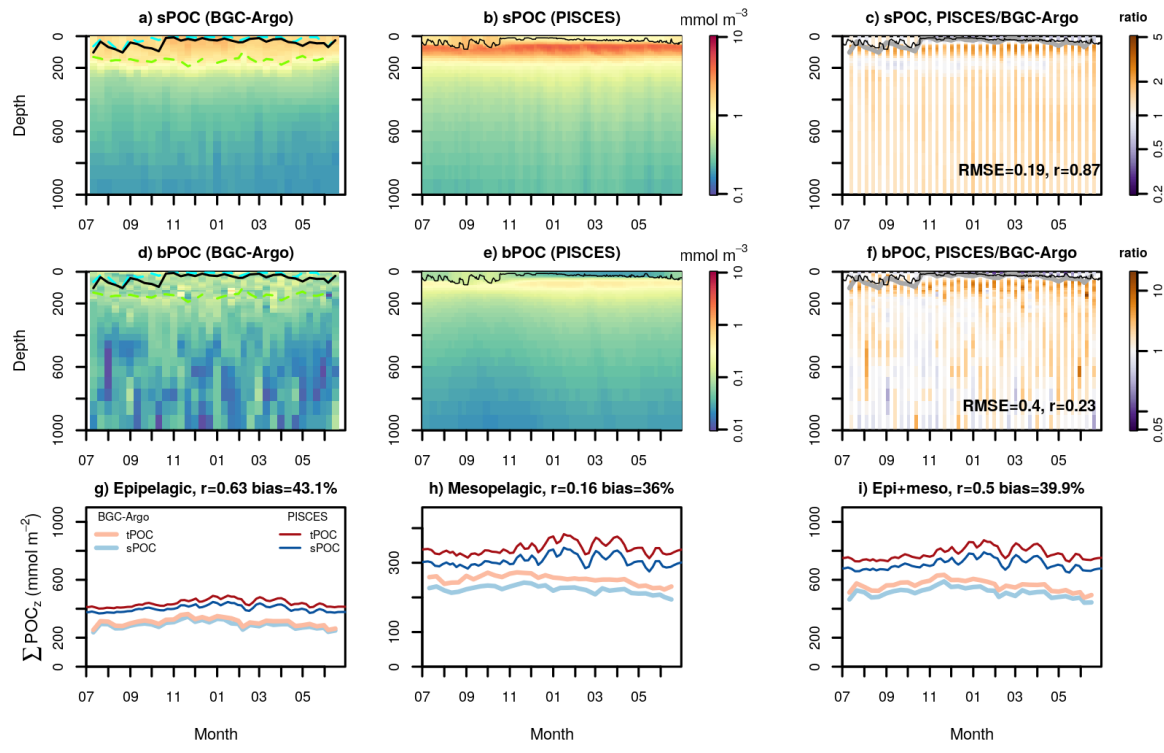


Figure S16. Alternative version of Fig. 7 of the main text including heterotrophic prokaryotes' biomass (*BACT*) diagnosed within PISCES using a simple empirical relationship.

Supplemental tables

Table S1. List of coherent annual time series (CATS) and their correspondence with ORCA1 grid cells where PISCES 1D simulations were run. This list is linked to the repository <https://doi.org/10.5281/zenodo.5139602>.

Biome	Subregion or basin	Float WMO	Year	Grid cell #
NASPG	Labrador Sea	6901480	2015	84220
			2016	84222
		6901486	2015	83138
		6901524	2014	83866
			2016	82061
		6901527	2014	83858
			2015	84586
		6901527	2016	83504
	Iceland Basin	6901516	2014	81705
		6901516	2015	82432
		6901647	2015	85335
		6901647	2016 ^a	85343
Mediterranean	NW Med.	6901648	2015	74865
	SW Med.	6901513	2014	73418
	Tyrrhenian Sea	6901491	2014	74147
	Ionian Sea	6901510	2014	72708
		6901529	2014	74155
	Levantine Sea	6901528	2014	71269
		6901764	2016	71993
			2017	71994
		6901765	2016	72348
			2017	72710
		6901766	2016	72355
			2018	71270

		6901768	2016	73432
			2017	72706
		6901773	2017	71634
			2018	71274
STG	North Atlantic STG	6901472	2013	66496
			2014	66495
			2015	66496
			2016	66493
			2017	65768
	South Pacific STG	6901658	2015	41020
			2016	41736
		6901660	2015	41032
			2016	40676
			2017	41040
		6902701	2016	40323
			2017	39601
		6902740	2017	39718
Subantarctic	Indian sector	6901574	2015	26421
		6901579	2015	26419
		6901580	2015	26079
		6901581	2015	26804
			2016	24665
	Atlantic to Indian sector	6901583	2015	27843
			2016	27520
			2017	27547
		6901585	2015	25658
			2016	23491